

Supplementary Materials

1. Materials.

Isopropyl alcohol (99.7%), glycerol (99%), iron (III) nitrate nonahydrate (98.5%), Nickel chloride hexahydrate ($\text{NiCl}_2 \cdot 6\text{H}_2\text{O}$) (98%), 4-nitrophenol (99%), methylene orange (MO), Congo red (CR) sodium borohydride (96%) were purchased from Sinopharm Chemical Reagent Co., Ltd. (Shanghai, China). Potassium tetrachloropalladate (K_2PdCl_4) was procured from Aladdin Chemistry Co., Ltd. (China). Deionized water (resistivity $> 18 \Omega \cdot \text{cm}^{-1}$) was used for all synthesis and experiments.

2. Characterization

The morphology and structure of the products were characterized by scanning electron microscopy (SEM, VEGA 3, Tescan) and transmission electron microscopy (STEM) Aberration-corrected scanning transmission electron microscopy (AC-STEM) images were acquired by using FEI Titan 80-300 equipped with a probe spherical aberration corrector and a monochromator at 300 kV. HAADF-STEM images were acquired with the illumination semi-angle of 25 mrad and probe current of 100 pA. The collection angles for the HAADF-STEM images were 120–250 mrad. The dwell time for image acquisition was set at 10 μs per pixel to ensure a desirable signal to noise ratio. The metal content of the prepared catalysts was determined with an inductivity coupled plasma-mass spectrometer (ICP-MS, Agilent 7700X, USA). The powder X-ray diffraction (XRD) patterns were recorded on a Cu ($K\alpha$) X-ray diffractometer ($\lambda = 1.5406 \text{ \AA}$) (Philips PW-1830, Netherlands), in which the step size and scan rate were set as $5^\circ/\text{min}$, respectively. The X-ray photoelectron spectrum (XPS) was tested on an ESCALAB MKII spectrometer (VG Co., UK), using Mg $K\alpha$ radiation (1253.6 eV) at a pressure of 2.0×10^{-10} mbar. The specific surface area was measured with Micromeritics ASAP2020. The SSA and porous size were calculated according to the Brunauer-Emmett-Teller (BET) and Barrett-Joyner-Halenda (BJH) methods, respectively. The UV-Vis spectra were measured with a UV-vis spectrophotometer (UV-2550, Shimadzu, Japan).

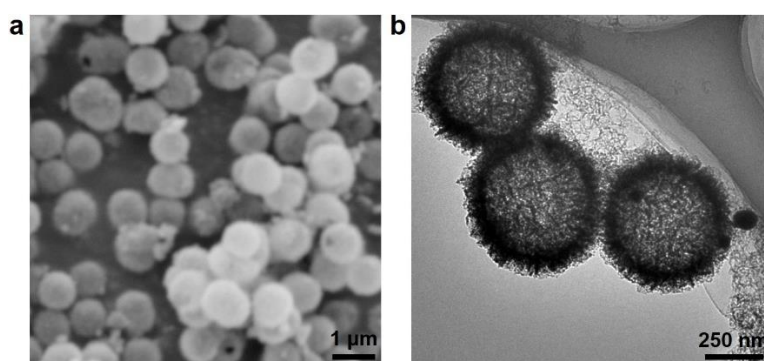


Figure S1 (a) SEM image and (b) TEM image of pristine Fe_3O_4 nanospheres.

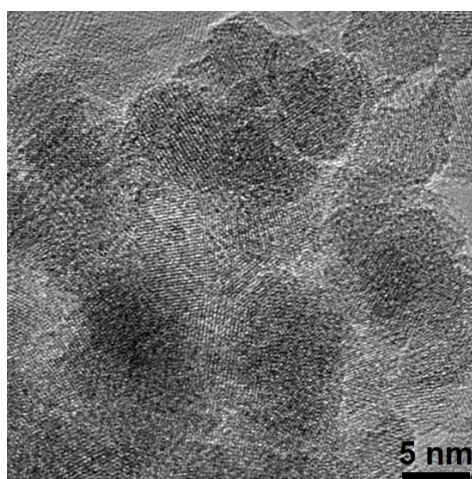


Figure S2 High-resolution TEM image of Ni-Pd/Fe₃O₄ catalyst.

3. Reduction reaction equations

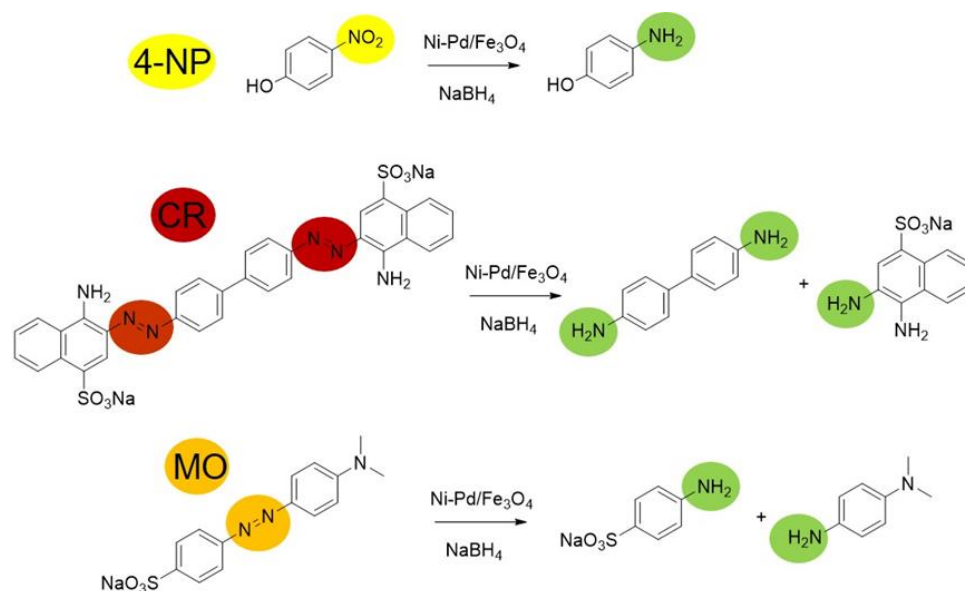


Figure S3. Catalytic reduction reaction equations of 4-NP, CR, and MO by NaBH₄ in the presence of Pd/Fe₃O₄ catalyst.

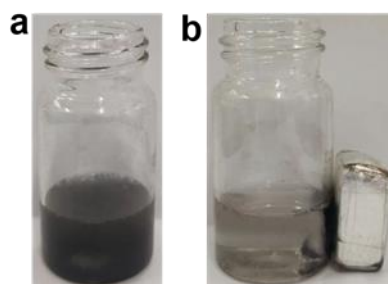


Figure S4. Photographs that illustrate the catalytic reduction process of 4-NP aqueous solution in the presence of Ni-Pd/Fe₃O₄ catalyst (a) and the easy recyclability of Ni-Pd/Fe₃O₄ catalyst by a magnet.

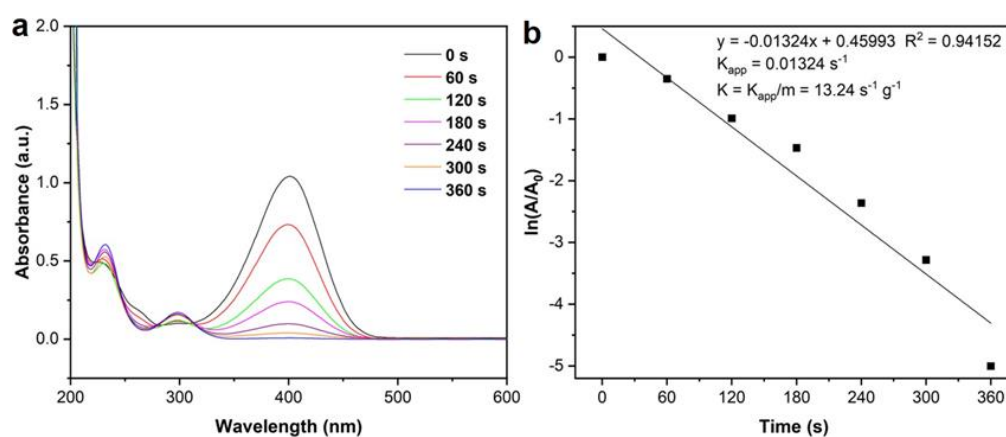


Figure S5. (a) Time-dependent UV-vis spectra for 4-NP reduction by NaBH₄ in the presence of Pd/Fe₃O₄ catalyst and (b) the corresponding rate constant versus time.

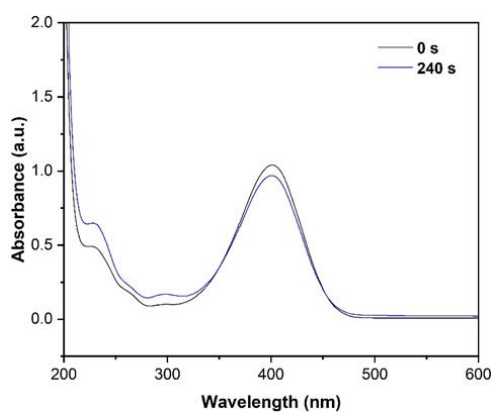


Figure S6. UV-vis spectra for 4-NP reduction by NaBH₄ in the presence of Ni/Fe₃O₄ for 4 min.

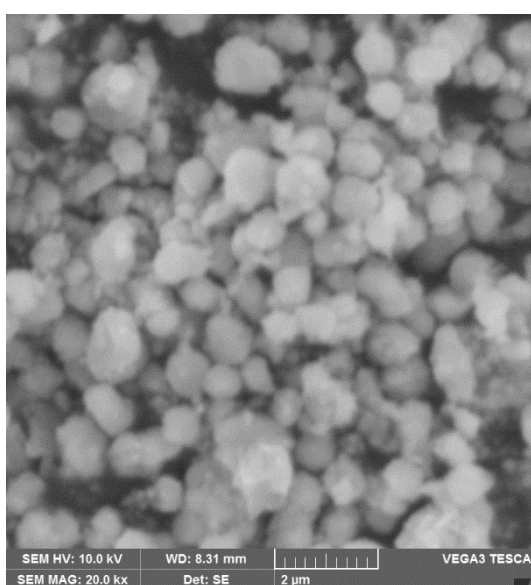


Figure S7 SEM image of the recycled Fe₃O₄ yolk-shelled nanospheres.

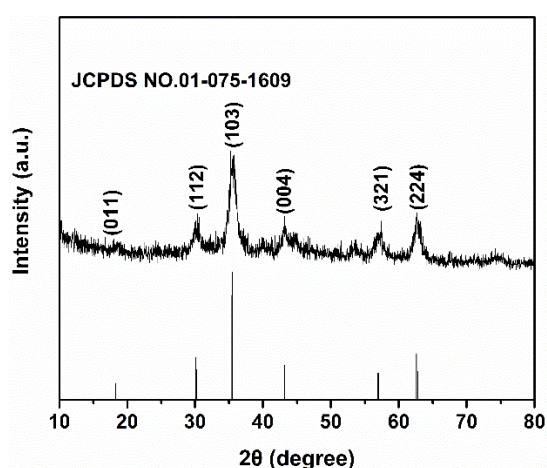


Figure S8 XRD pattern of recycled Ni-Pd/Fe₃O₄ and standard card JCPDS No. 01-075-1609.

Table S1 Comparison of the turnover frequency (TOF) in the 4-NP reduction catalyzed by the Fe₃O₄ supported catalysts in this work and the reported literature.

| $\text{HO}-\text{C}_6\text{H}_4-\text{NO}_2 \xrightarrow[\text{Catalyst}]{\text{NaBH}_4} \text{HO}-\text{C}_6\text{H}_4-\text{NH}_2$ | | | | | |
|--|-----------------------|-----------------------|----------------------|----------------------------------|-----------|
| Catalyst | Mass of catalyst (mg) | Amount of 4-NP (mmol) | Conversion time(min) | TOF (mmol 4-NP/(mmol metal min)) | Ref. |
| Pd-Ni/Fe ₃ O ₄ | 1 | 1×10 ⁻¹ | 4 | 295 ^a | This work |
| Pd/Fe ₃ O ₄ | 1 | 1×10 ⁻¹ | 6 | 204 | This work |
| Ni/Fe ₃ O ₄ | 1 | 1×10 ⁻¹ | - | - | This work |
| Pd-Fe ₃ O ₄ | 3 | 6×10 ⁻² | 1.83 | 145 | [35] |
| Fe ₃ O ₄ @PDA/Au/PDA | 3 | 5×10 ⁻³ | 5 | 0.7 | [48] |
| Fe ₃ O ₄ @CS_AgNi | 0.4 | 0.25×10 ⁻³ | 10 | 0.008 | [49] |
| Fe ₃ O ₄ /SiO ₂ @PDA/Pd | 2 | 3×10 ⁻³ | 2 | 4.3 | [50] |
| Fe ₃ O ₄ @MIL-100(Fe)/Ag | 0.1 | 3×10 ⁻⁴ | 1 | 45 | [51] |
| Fe ₃ O ₄ @C@Au | 1 | 1×10 ⁻⁴ | 0.67 | 0.13 | [52] |
| Cu/MC | 0.5 | 1.8×10 ⁻³ | 5 | 0.91 | [53] |
| Ag/C/Fe ₃ O ₄ | 6 | 7.5×10 ⁻² | 7 | 2.3 | [54] |

| | | | | | |
|--|--------------------|----------------------|------|-------|------|
| Fe ₃ O ₄ @Alg-AuNPs | 1 | 7.5×10 ⁻³ | 4 | 10.26 | [55] |
| Fe ₃ O ₄ @COF-Au | 3 | 9×10 ⁻³ | 20 | 5.8 | [56] |
| Ag@Fe ₃ O ₄ | 0.1 | 3×10 ⁻⁴ | 8 | 0.04 | [57] |
| Fe ₃ O ₄ /SiO ₂ -NH ₂ @CS/Pd | 23 | 7.5×10 ⁻³ | 2 | 0.54 | [58] |
| Au/Fe ₃ O ₄ | 1 | 5×10 ⁻⁴ | 0.33 | 13.8 | [59] |
| 10Ag-FA | 20 | 5×10 ⁻³ | 5 | 0.09 | [60] |
| Co-Fe ₃ O ₄ @C-A | 0.1 | 3×10 ⁻⁴ | 1.33 | 3.43 | [61] |
| Cu-APTES@Fe ₃ O ₄ | 3×10 ⁻² | 5×10 ⁻⁴ | 10 | 4.18 | [62] |
| CNT/PdFe/NC | 3 | 6×10 ⁻² | 2.5 | 16.7 | [63] |
| PDA-g-C ₃ N ₄ /Au | 5 | 3×10 ⁻³ | 1.3 | 7.0 | [64] |
| Pd/GNS-NH ₂ | 5 | 2×10 ⁻² | 1 | 41.7 | [65] |
| Pd/Pr ₆ O ₁₁ | 0.14 | 1×10 ⁻³ | 3 | 17.8 | [66] |

^a Calculated based on active metal Pd.